Nanotechnology **22** (2011) 015301 (6pp) doi:10.1088/0957-4484/22/1/015301

Electron-beam-induced deposition of gold from aqueous solutions

G Schardein, E U Donev and J T Hastings

Department of Electrical and Computer Engineering and Center for Nanoscale Science and Engineering (CeNSE), University of Kentucky, Lexington, KY 40506, USA

E-mail: hastings@engr.uky.edu

Received 30 June 2010, in final form 13 August 2010
Published 6 December 2010
Online at stacks.iop.org/Nano/22/015301

Abstract

Focused electron-beam-induced deposition (EBID) using bulk liquid precursors is a novel approach to nanofabrication that has shown improvements in purity compared to EBID with gas-phase precursors. Here we report the first EBID of gold using bulk liquid precursors. We study the differences in gold deposited from three different aqueous solutions containing chloroauric acid ($HAuCl_4$), sodium tetrachloroaurate ($NaAuCl_4$), and the disulfitoaurate complex ($[Au(SO_3)_2]^{3-}$). We also examine the dependence of threshold dose upon precursor concentration and demonstrate high-resolution patterning with a pitch as small as 50 nm. Finally, we show that the purity of gold deposited using these liquid precursors is significantly improved in comparison with deposits from metal–organic gaseous precursors.

1. Introduction

Focused electron-beam-induced deposition (EBID) is becoming increasingly important within the nanotechnology community. The process has proven useful in a wide array of applications ranging from nanoscale device prototyping to lithographic mask repair [1]. Though the majority of EBID to date has been based on gas-phase (GP) precursors, we have recently investigated EBID using bulk liquid precursors. Specifically, we reported platinum deposition from an aqueous solution of chloroplatinic acid that showed marked improvement over gas-phase processes in terms of deposition purity. This process yielded dense, high-resolution deposits (25 nm lines and dots at 60 nm pitch) [2] with purity exceeding 85 at.% [3]. Liquid precursors also offers other advantages including the use of less toxic and expensive chemistry, the dissipation of charge in the conductive solution, and the potential to increase deposition rates.

Other groups have also investigated electron-beam-induced reactions in liquids. In one variation of gas-phase EBID, the gaseous or liquid precursor can be condensed on a cooled substrate as reported by Mitchell and Hu [4]. Work has also been conducted to synthesize nanomaterials by electron-beam bombardment of liquids. In this case, the nanostructures are produced over a large area with quasi-random distributions. Two silver deposition processes have been investigated based on the large area electron-beam bombardment of either aqueous solutions [5] or ionic-liquid solution [6]. The former process produced randomly distributed nanoparticles and the latter produced dendritic structures. Similarly, electron-beam-induced gold nanoparticles synthesis has been explored using ionic liquids and both low (10 keV) [7] and high (4.8 MeV) [8] energy electron beams. However, none of these processes sought to fabricate user-designed nanopatterns such as those produced here.

Here we extend our investigation of liquid-phase (LP) EBID by exploring bulk liquid precursors for gold deposition. The numerous applications of gold in electronics and photonics provide strong motivation to identify a LP process similar to that for platinum. Moreover, current gas-phase processes for gold deposition using metal–organic precursors yield highly contaminated deposits [9]. A custom synthesized gaseous precursor for gold (chlorotrifluorophosine) yielded purity greater than 90 at.% Au; however, the lack of commercial availability, chemical instability, and difficulty in handling this precursor also motivates the search for an alternative. Here we demonstrate LP-EBID from three gold precursors with varying concentration in aqueous solution. We also report the threshold dose required to initiate deposition from the more promising solutions. Finally, we assess the purity of the gold deposits and place this in the context of gas-phase precursors.

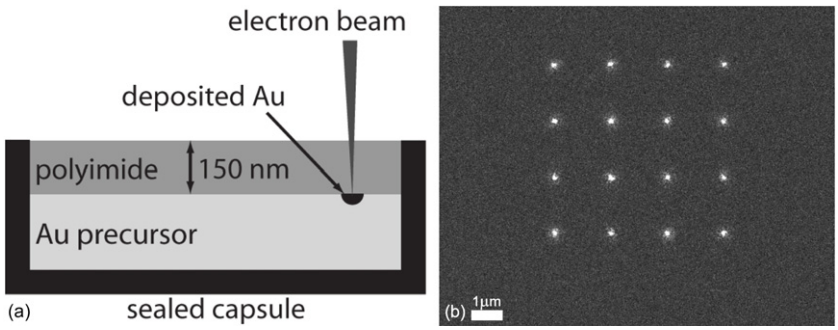

Figure 1. (a) Schematic of liquid-phase electron-beam-induced deposition (LP-EBID) of gold using an aqueous solution as a precursor. The solution is separated from the vacuum system by a polyimide membrane and the electron beam is focused at the membrane–solution interface to induce deposition. (b) *In situ* electron micrograph of Au nanodots deposited by LP-EBID using a 100 mM $[Au(SO_3)_2]^{3-}$ solution. The dose is 25 pC/dot and the scale bar indicates 1 μm.

2. Experimental details

Depositions were carried out using QuantomiX QX-102 WETSEM capsules that use a ∼150 nm thick polyimide membrane to separate the liquid from the vacuum [10]. Deposits were created by focusing the electron beam at the interface between the liquid precursor and the bottom of the membrane as shown in figure 1. Charging of the polyimide membrane is not a problem because the conductive precursors dissipate excess charge (though this may be a future consideration if one wishes to minimize pattern placement and critical dimension errors). Colloidal gold particles were placed on the vacuum side of the membrane to be used as focusing artifacts. For most cases, 200 nm particles sufficed while 50 nm particles were used for the higher-resolution patterns.

The first precursor used for deposition was chloroauric acid ($HAuCl_4$), which is similar in composition to the precursor used in the previously reported platinum process (H_2PtCl_6). In solution, deposition proceeds from the chloroaurate ion ($[AuCl_4]^-$). For chloroauric acid experiments the concentration was varied logarithmically from 0.01 to 10 mM to find a concentration that provided well defined patterns. Two other precursors were also investigated, $NaAuCl_4$ (a neutral source for the chloroaurate ion) as well as a solution of $NaAuCl_4$ and Na_2SO_3 which forms the disulfitoaurate complex ($[Au(SO_3)_2]^{3-}$) commonly used in gold electrodeposition [11]. Solutions containing $[Au(SO_3)_2]^{3-}$ were prepared by dissolving a given concentration of $NaAuCl_4$ along with Na_2SO_3 at 10× that concentration. All precursor solutions were prepared using deionized water (18 MΩ), and all chemicals were obtained from Sigma-Aldrich and used as received.

The exposed patterns and exposure conditions were chosen to determine the required threshold dose for each precursor. For the $HAuCl_4$ solutions, we exposed arrays of single-pixel dots with 2 μm spacing and doses ranging from 1 to 350 pC/dot. The same dose matrix was tested for the neutral $NaAuCl_4$ precursor. However, for $[Au(SO_3)_2]^{3-}$, larger doses were necessary to create detectable deposits and 2 μm spaced 250–450 pC/dot patterns were used in addition to the standard dose matrix.

For all three precursors, denser patterns were created for compositional analysis using energy-dispersive x-ray spectroscopy (EDS). For $HAuCl_4$, the pattern was a 5 μm × 5 μm array of dots spaced by 200 nm and with a constant dose of 30 pC/dot while for $[Au(SO_3)_2]^{3-}$, a less dense array of 1 μm spaced dots was used with doses ranging from 350 to 450 pC/dot. Also, for the $[Au(SO_3)_2]^{3-}$ solution, high-density patterns were created to determine the highest resolution that could be obtained. In all cases, deposition was performed using a primary beam energy of 20 keV and a beam current of approximately 200 pA in a Raith e_LiNE electron-beam lithography tool.

After each pattern was created, scanning electron micrographs (SEMs) were immediately taken *in situ*. Finally, the denser patterns were analyzed by EDS on a Hitachi S-3200 SEM. Monte Carlo electron trajectory simulations were conducted with CASINO [12] using the default physical models and a semi-infinite water layer. To assess the reliability of the simulations, we compared the calculated backscattering coefficient from water at 20 keV (0.055) with Joy's experimental value (0.042) [13] and found relatively good agreement.

3. Results and discussion

Figure 2 shows dose matrices patterned using 0.01–1 mM aqueous $HAuCl_4$ solutions. For low concentrations (0.01 mM), deposits were incomplete. For higher concentrations (1 mM), deposits were much more uniform and complete throughout the dose array. However, for 1 mM solutions there was a large amount of 'collateral deposition' where gold was deposited *en masse* throughout and around the dose matrix pattern. This phenomenon is most likely due to backscattered electrons (BSE) nucleating gold deposition away from the target area.

To test this hypothesis we compared the backscattered electron range from water, calculated using Monte Carlo simulation, to the observed range for collateral deposition [12]. As shown in figure 2(d), the number of backscattered electrons from water for a given radius peaks near 3 μm and falls off rapidly beyond 4 μm. This is consistent with figure 2(c) where the range of collateral deposition is observed to be approximately 4 μm.

For the intermediate concentration of 0.1 mM, we found that deposits are compact with limited collateral

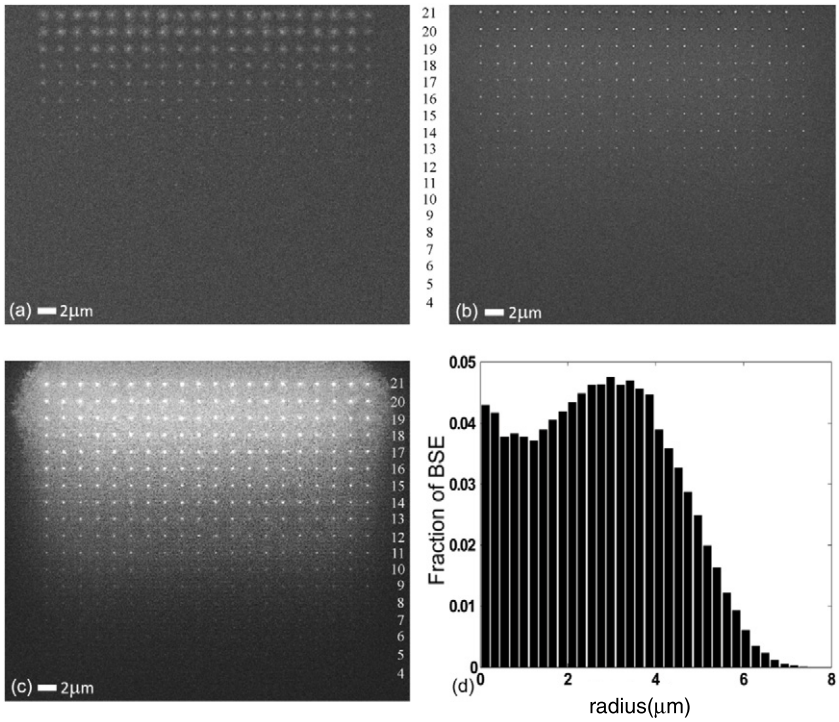

Figure 2. Dose array of Au nanodots (2 μm pitch) deposited via LP-EBID using $HAuCl_4$ as a precursor, at a concentration of (a) 0.01 mM, (b) 0.1 mM, and (c) 1 mM. Doses for rows 4, 5–9 (in pC/dot): 7, 10–50 by 10. Doses for rows 10–21 (in pC/dot): 75–350 by 25. Note that for lower concentrations, deposition is incomplete while at higher concentrations there is significant collateral deposition in unexposed regions. (d) Calculated backscattered electron (BSE) radial distribution for a 20 keV electron beam incident on water. Each bar represents the fractions of electrons emerging in a 220 nm wide ring at the given radius. The distribution peaks near 3 μm and falls off rapidly beyond 4 μm, in good agreement with the range of collateral deposition experimentally observed in the figure.

deposition. This indicates that maintaining reliable deposition of gold while minimizing collateral deposition requires careful selection of precursor concentration. The threshold dose required to initiate deposition is approximately 75 pC/dot for 0.1 mM $HAuCl_4$ and 40 pC/dot for 1 mM $HAuCl_4$. This suggests that threshold dose decreases with increasing precursor concentration.

Next, figure 3 shows deposits from a 1 mM aqueous $NaAuCl_4$ solution. Collateral deposition is once again evident at higher doses. Dot diameter also appears to depend more strongly on dose when compared to the 1 mM $HAuCl_4$ deposits (cf, figure 2(c)). Threshold dose is reduced to 7 pC compared to the 1 mM $HAuCl_4$ solution.

Figure 4 shows deposits from 0.1 and 1 mM $NaAuCl_4$ solutions with Na_2SO_3 added at 10× the $NaAuCl_4$ concentration. Thus the deposition primarily proceeds from the $[Au(SO_3)_2]^{3-}$ ion [14, 15]. As with the other two solutions, at 0.1 mM concentration we see little evidence of collateral deposition. The threshold dose is estimated to be 125 pC/dot for 0.1 mM and 50 pC/dot for 1 mM solutions. In both cases this dose is higher than the corresponding doses for the chloroaurate precursors at the same concentrations.

Furthermore, even for the 1 mM $[Au(SO_3)_2]^{3-}$ solution, collateral deposition is much less evident than for the deposits from either 1 mM $HAuCl_4$ or 1 mM $NaAuCl_4$ alone. This suggests that the backscattered electron dose is insufficient to nucleate deposits away from the targeted region even at this high concentration. This observation is consistent with the higher threshold dose required for deposition from the disulfitoaurate complex compared to the chloroaurate complex.

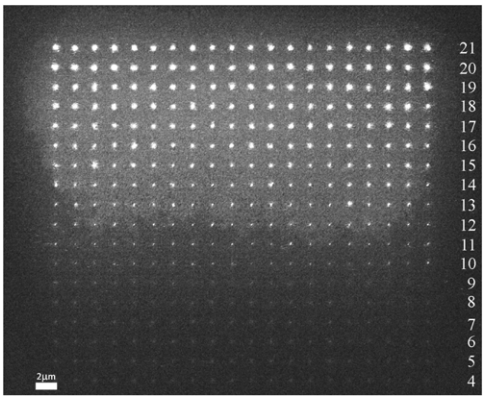

Figure 3. Dose array of Au nanodots (2 μm pitch) deposited via LP-EBID using 1 mM $NaAuCl_4$ as a precursor. Doses for rows 4, 5–9 (in pC/dot): 7, 10–50 by 10. Doses for rows 10–21 (in pC/dot): 75–350 by 25. Morphology of the deposits and collateral deposition are similar to those observed for $HAuCl_4$.

Finally, high-resolution and high-density patterns were created using the disulfitoaurate solution with 0.1 mM $NaAuCl_4$ and 1 mM Na_2SO_3. Dot matrices with pitches as small as 50 nm were patterned at a dose of 4 pC/dot. As shown in figure 5, collateral deposition remains an issue for high-density features; however, distinct dots are discernable

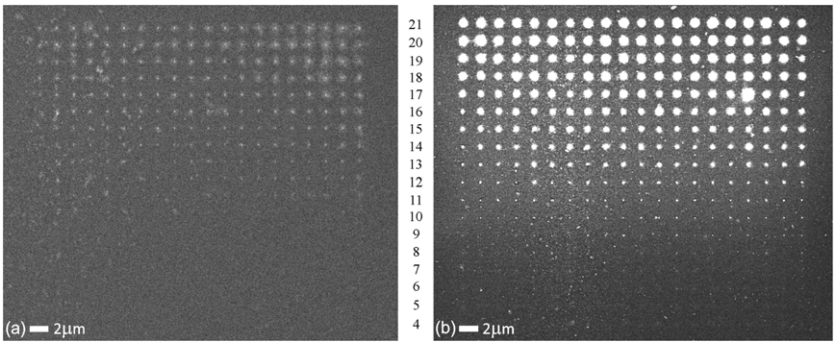

Figure 4. Dose array of Au nanodots (2 μm pitch) deposited via LP-EBID using $[Au(SO_3)_2]^{3-}$ as a precursor, at a concentration of (a) 0.1 mM and (b) 1 mM. Doses for rows 4, 5–9 (in pC/dot): 7, 10–50 by 10. Doses for rows 10–21 (in pC/dot): 75–350 by 25. Note that for higher concentrations, collateral deposition seems to be reduced (cf, figures 2(c) and 3).

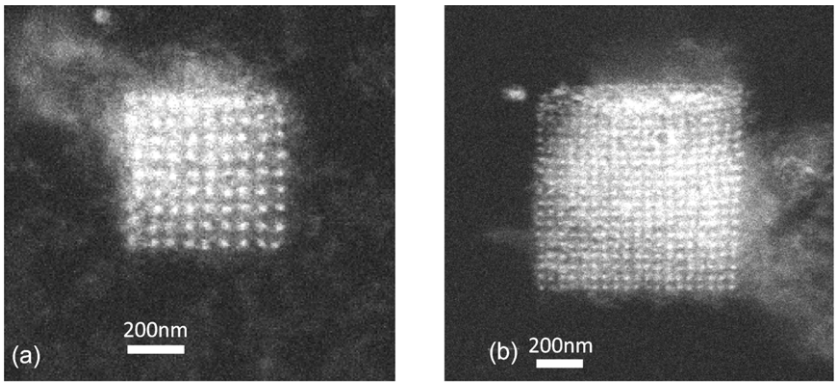

Figure 5. High-resolution patterns using $[Au(SO_3)_2]^{3-}$ from solution of 0.1 mM $NaAuCl_4$ and 1 mM Na_2SO_3. (a) 9 × 9 array of Au nanodots at a dose of 10 pC/dot with 70 nm pitch. (b) 19 × 19 array of Au nanodots at a dose of 4 pC/dot with 50 nm pitch.

even at 50 nm pitch (figure 5(b)). In addition to collateral deposition within the pattern, there also appears to be an additional, 'hazy' deposit located nearby. The asymmetry and nonuniformity of this deposition suggests the presence of another mechanism apart from reduction by backscattered electrons. Though the deposits were not as clean as those seen from LP-EBID of platinum [2], these results suggest similar resolution may indeed be possible with gold-based precursors if collateral deposition can be controlled.

In order to estimate the purity of our Au deposits, we performed energy-dispersive x-ray spectroscopy (EDS) measurements and simulations. Experimental EDS was done on a Hitachi S-3200 SEM operating at 20 keV, after the liquid precursor had been removed and the capsule reservoir aspirated several times with deionized water and dried in air. For the Monte Carlo simulations, we used NIST's DTSA-II software package for quantitative x-ray microanalysis [16].

Trace 3 in figure 6 (upper panels) corresponds to an experimental spectrum of the bare polyimide membrane, i.e. collected from an area with no deposits. Apart from prominent carbon (C) and oxygen (O) peaks, and a weak but discernible nitrogen (N) peak, all of which can be attributed to the constituent elements of generic polyimide, we observe a small peak at 1.75 keV attributable to silicon (Si). Most of the Si signal likely originates from (i) autofluorescence of the 'dead layer' at the entrance face of the Si detector crystal [17], with possible additional contributions from (ii) the area of the stainless-steel sample holder situated a few millimeters directly below the electron-transparent polyimide membrane and/or from (iii) the stainless-steel grid supporting the membrane. The other two experimental EDS spectra (figure 6 (upper panels)) also show evidence of a Si peak, here convolved with the nearby gold (Au) peak at 1.65 keV. The simulated spectrum of a specific polyimide film (DuPont's Kapton®: $C_{22}H_{10}N_2O_5$) is plotted as trace 7 in figure 6 (lower panels) for comparison; C, N, and O peaks are clearly visible.

Traces 1 and 2 in figure 6 (upper panels) correspond to experimental EDS spectra obtained from gold-covered areas of polyimide membranes, deposited by LP-EBID from an acidic chloroaurate solution ($HAuCl_4$, trace 2) or from a disulfitoaurate solution ($NaAuCl_4$ + Na_2SO_3, trace 1). In addition to multiple Au peaks, several other peaks can be identified in both experimental spectra: C, N, and O peaks due to the supporting membrane; the convolved Si artifact discussed above; chromium (Cr), iron (Fe), and nickel (Ni) artifacts from the stainless-steel sample holder and/or support grid. However, only the spectrum for the $HAuCl_4$ case exhibits a chlorine (Cl) shoulder near 0.18 keV, on the low-energy side of the C peak, along with a small Cl bump at 2.62 keV.

To estimate the amount of Cl contamination in our Au deposits, we cross-compare the experimental data with the

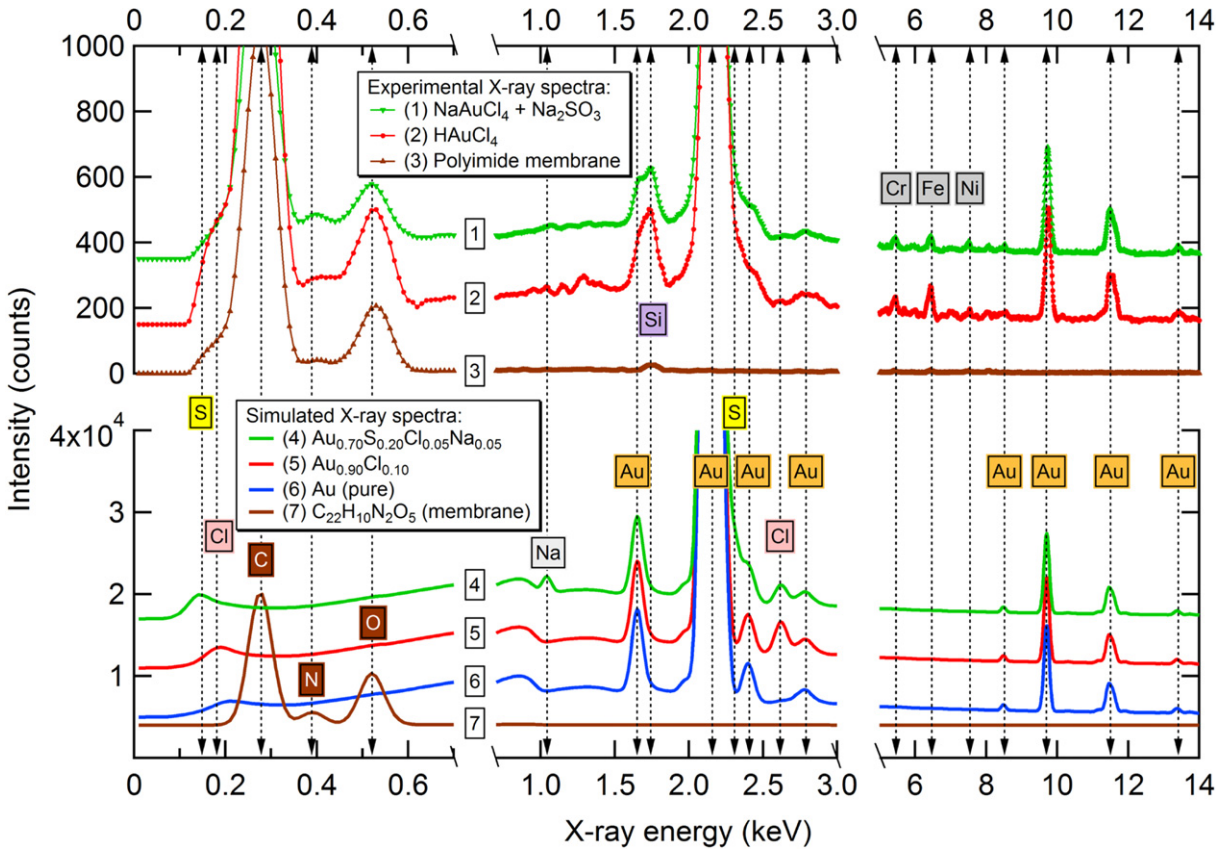

Figure 6. (Upper panels) Experimental energy-dispersive x-ray spectra (EDS) of gold (Au) patterns deposited via LP-EBID from aqueous solutions of 0.1 mM chloroauric acid ($HAuCl_4$, trace 2) and 0.1 mM sodium tetrachloroaurate with 1.0 mM sodium sulfite ($NaAuCl_4 + Na_2SO_3$, trace 1), along with a spectrum of the bare polyimide membrane supporting the deposits (trace 3). (Lower panels) Simulated EDS spectra of a free-standing (150 nm thick) polyimide film ($C_{22}H_{10}N_2O_5$, trace 7) and three free-standing (100 nm thick) Au films with varying atomic fractions of sulfur (S), chlorine (Cl), and sodium (Na) impurities, i.e.: none (100 at.% Au, trace 6), 10 at.% Cl (trace 5), and 20 at.% S + 5 at.% Cl + 5 at.% Na (trace 4). All Au-containing traces are offset vertically for clarity and normalized to the highest Au peak (2.12 keV), which is truncated in the plots for better visualization of impurity peaks. Horizontal axes are truncated for clarity and to exclude a region (3–5 keV) with no observable peaks. Energy positions of characteristic x-ray peaks are marked by vertical dotted lines and labeled with corresponding element symbols.

(This figure is in colour only in the electronic version)

simulated spectra of a pure Au film (trace 6 in figure 6 (lower panels)) and two impure Au films containing 10 at.% Cl (trace 5) and 5 at.% Cl (trace 4). Judging by the relative heights of the Au and Cl peaks within each spectrum, we can place an upper bound of 5 at.% Cl contamination for Au deposits from either precursor.

The quantification of sulfur (S) contamination is more difficult because the main S peak at 2.31 keV partially overlaps with a much more intense Au peak, while the secondary S peak at 0.15 keV falls near the low-energy cutoff of the EDS detector. Nevertheless, we place a conservative upper bound of 20 at.% S contamination for the Au structures deposited from the $NaAuCl_4$+Na_2SO_3 precursor, suggested by: (i) the absence of a pronounced sulfur shoulder on the low-energy side of the C peak (near 0.15 keV), in contrast to the Cl shoulder (near 0.18 keV) in the $HAuCl_4$ case; and (ii) the similarity in shape of the shoulder on the high-energy side of the main Au peak (2.25–2.50 keV) in the experimental spectra for both precursors, even though one of them ($HAuCl_4$) nominally does not contain sulfur.

As for sodium (Na), the experimental peaks near 1.04 keV are too small for positive identification, but we still assign a maximum Na concentration of 5 at.% for the sake of completeness. For overall comparison, a simulated spectrum of an impure Au film containing the maximum estimated fractions of all three nominal contaminants—20 at.% S, 5 at.% Cl, and 5 at.% Na—is plotted as trace 4 in figure 6 (lower panels).

To place these results in context, consider the purity of electron-beam-induced deposition from gas-phase Au precursors. A complete comparison with the available Au precursors and deposition conditions is beyond the scope of this discussion, but can be found in the review by Botman *et al* [9]. Most metal–organic gold precursors yield 5–25 at.% gold in a mostly carbonaceous deposit. Notable exceptions to this include the combination of a metal–organic precursor with a mixture of Ar/O_2 to achieve 50 at.% Au [18] and the use of a highly unstable (few hours in contact with metal) and not commercially available chlorotrifluorophosine precursor ($AuClPF_3$) that deposits partially interconnected gold grains with >90 at.% purity [19]. In contrast, we have achieved

>95 at.% gold from readily available, easily handled, and inexpensive aqueous solutions.

4. Conclusions

We have reported the first *focused* electron-beam-induced deposition of gold from aqueous solutions. Both acidic and neutral solutions containing $[AuCl_4]^-$ ions yield similar deposits with a small variation in threshold dose. Deposition is dependent upon precursor concentration and optimal results were obtained with 0.1 mM $HAuCl_4$ solutions. At lower concentrations, gold fails to deposit uniformly, while at higher concentrations we observe significant collateral deposition, which we attribute mainly to electrons backscattered from the solution. However, asymmetric deposition near higher-density patterns suggests that more than one mechanism of collateral deposition may be involved. For gold deposition from the 0.1 mM $[Au(SO_3)_2]^{3-}$ complex we obtained patterns similar to those from the 0.1 mM $[AuCl_4]^-$ solutions, whereas collateral deposition from 1 mM $[Au(SO_3)_2]^{3-}$ was significantly reduced compared to 1 mM $[AuCl_4]^-$.

Perhaps most importantly, gold deposits from both types of liquid precursors showed much improved purity compared to deposits from the metal–organic precursors typically used in gas-phase EBID. The purity of deposits from $HAuCl_4$ solutions (<5 at.% Cl contamination) is at least comparable to deposits formed from the highly unstable and commercially unavailable chlorotrifluorophosine gas precursor [19]. Distinct patterns with a half-pitch of 25 nm were obtained in this work, although collateral deposition limits their utility for many applications. A goal for future work is to identify liquid precursors for gold that further reduce collateral deposition. In the meantime, liquid-phase e-beam-induced deposition (LP-EBID) continues to provide a rapid means to deposit high-resolution patterns composed of high-purity materials.

Acknowledgments

This work was partially supported by the Kentucky Science and Engineering Foundation under Grant KSEF-148-502-08-240. This material is also partially based upon work supported by the Defense Advanced Research Projects Agency under Award No. N66001-09-1-2099. Any opinions, findings, and conclusions or recommendations expressed in this publication are those of the authors and do not necessarily reflect the views of the Defense Advanced Research Projects Agency. The authors thank Larry Rice for his technical assistance with the EDS measurements as well as Brian Wajdyk at Center for Nanoscale Science and Engineering for assistance with the e-beam system.

References

[1] Silvis-Cividjian N and Hagen C W 2006 *Adv. Imaging Electron Phys.* **143** 1–235
[2] Donev E U and Hastings J T 2009 Liquid-precursor electron-beam-induced deposition of Pt nanostructures: dose, proximity, resolution *Nanotechnology* **20** 505302
[3] Donev E U and Hastings J T 2009 Electron-beam-induced deposition of platinum from a liquid precursor *Nano Lett.* **9** 2715–8
[4] Mitchell W J and Hu E L 2002 High-resolution *in situ* electron beam patterning using $Ti(OC_3H_7)(4)$ as a negative-type resist *J. Vac. Sci. Technol.* B **20** 596–603
[5] Pai Y H and Lin G R 2010 *In situ* synthesis of scalable metallic nanodots in electron microscope *J. Electrochem. Soc.* **157** E13–8
[6] Roy P, Lynch R and Schmuki P 2009 Electron beam induced in-vacuo Ag deposition on TiO_2 from ionic liquids *Electrochem. Commun.* **11** 1567–70
[7] Imanishi A, Tamura M and Kuwabata S 2009 Formation of Au nanoparticles in an ionic liquid by electron beam irradiation *Chem. Commun.* 1775–7
[8] Tsuda T, Seino S and Kuwabata S 2009 Gold nanoparticles prepared with a room-temperature ionic liquid-radiation irradiation method *Chem. Commun.* 6792–4
[9] Botman A, Mulders J J L and Hagen C W 2009 Creating pure nanostructures from electron-beam-induced deposition using purification techniques: a technology perspective *Nanotechnology* **20** 372001
[10] Thiberge S, Zik O and Moses E 2004 An apparatus for imaging liquids, cells, and other wet samples in the scanning electron microscopy *Rev. Sci. Instrum.* **75** 2280–9
[11] Green T A 2007 Gold electrodeposition for microelectronic, optoelectronic and microsystem applications *Gold Bull.* **40** 105–14
[12] Drouin D, Couture A R, Joly D, Tastet X, Aimez V and Gauvin R 2007 CASINO V2.42—a fast and easy-to-use modeling tool for scanning electron microscopy and microanalysis users *Scanning* **29** 92–101
[13] Joy D C and Joy C S 2006 Scanning electron microscope imaging in liquids—some data on electron interactions in water *J. Microsc.-Oxford* **221** 84–8
[14] Kato M and Okinaka Y 2004 Some recent developments in non-cyanide gold plating for electronics applications *Gold Bull.* **37** 37–44
[15] Liew M J, Sobri S and Roy S 2005 Characterisation of a thiosulphate-sulphite gold electrodeposition process *Electrochim. Acta* **51** 877–81
[16] Ritchie N W M 2010 *DTSA-II* Betelgeuse ed
[17] Reed S J B and Ware N G 1972 Escape peaks and internal fluorescence in x-ray-spectra recorded with lithium drifted silicon detectors *J. Phys. E: Sci. Instrum.* **5** 582
[18] Folch A, Servat J, Esteve J, Tejada J and Seco M 1996 High-vacuum versus an environmental' electron beam deposition *J. Vac. Sci. Technol.* B **14** 2609–14
[19] Brintlinger T, Fuhrer M S, Melngailis J, Utke I, Bret T, Perentes A, Hoffmann P, Abourida M and Doppelt P 2005 Electrodes for carbon nanotube devices by focused electron beam induced deposition of gold *J. Vac. Sci. Technol.* B **23** 3174–7